Laser-based interfacial patterning enables toughening of CFRP/epoxy joints through bridging of adhesive ligaments

Contents lists available at ScienceDirect

Composites Part A

journal homepage: http://ees.elsevier.com

Laser-based interfacial patterning enables toughening of CFRP/epoxy joints through bridging of adhesive ligaments

Ran Tao [a], Xiaole Li [a], Arief Yudhanto [a], Marco Alfano [b], Gilles Lubineau [a,*]

[a] King Abdullah University of Science and Technology (KAUST), Physical Sciences and Engineering Division (PSE), COHMAS Laboratory, Thuwal 23955-6900, Saudi Arabia
[b] Department of Mechanical, Energy and Management Engineering, University of Calabria, 87036 Rende, CS, Italy

ARTICLE INFO

Keywords
Bonding
CFRP
Bridging
Laser
Toughening strategy

ABSTRACT

The ability to prevent catastrophic failures in secondary bonded CFRP adhesive joints is important for reliable automotive and aerospace structures. In a previous study, we proposed an innovative damage-tolerant interfacial design concept for adhesively bonded composite joints, which relied on the extrinsic dissipation of bridging adhesive ligaments enabled by controlling the adhesion at CFRP/epoxy interfaces. In this work, we experimentally validate this strategy by combining laser processing and mechanical testing using double cantilever beam (DCB) joints. Mechanical tests indicate that the pattern geometry, *i.e.*, number and spacing of the areas with different adhesion, controls the formation of either single or multiple bridging adhesive ligaments. Therefore, the proposed strategy increases the overall work of fracture, and delay crack propagation by the associated tractions in the crack's wake, paving a promising route to design more reliable and safer CFRP adhesive joints.

1. Introduction

Carbon fiber-reinforced polymers (CFRPs) have been widely adopted in the aerospace and automotive industries [1,2]. However, joining primary composite structures remains a major challenge because of the mechanisms of multi-scale and complex damage [3,4]. State-of-the-art secondary adhesive bonding, in which the number of rivets or bolts is heavily reduced, is a promising strategy for joining CFRPs, due to the reduction in the total weight, a more integrated structure, and uniform stress distribution over the joint region [5–7]. Secondary adhesive bonding involves three components: the substrate, the adhesive, and the interface between them. As substrate and adhesive materials are usually determined by their specific engineering requirements, the interface is typically the component that is most readily modified to influence the mechanical response of the joint. The interface performance depends directly on the fabrication process and the surface pretreatment technique employed for bonding. Various pretreatments have been developed for composite substrates, such as peel ply, sandblasting, plasma treatment, and pulsed laser irradiation [8]; pulsed laser irradiation is of great interest due to its ability to selectively target the surface composition, topography and morphology. Apart from uniform modifications that promote chemical bonding and/or mechanical interlocking, advanced patterning strategies may also have a profound effect on the mechanical behavior of bonded joints [9–13]. By spatially modulating adhesion properties (surface chemistry or morphology), the obtained energy release rate (ERR) [11,13], the crack growth stability [14,15], and the crack propagation path [10,13] can be tuned and designed intentionally.

However, although work of fracture can be improved, the most important limitations when using secondary bonded joints are (*i*) the brittle response once a crack is initiated, and (*ii*) the difficulties in determining (by inspection) the occurrence of premature delaminations. Therefore, the widespread application of secondary bonded joints for critical load-bearing components is somewhat hampered. Several methods have been reported to delay or arrest crack propagation. For instance, substrate corrugations [16] and z-pinning or stitching [17–20] are efficient, but they require the modification of the structure before polymerization of the substrate, thus limiting their application in secondary bonding. Modifying or structuring the adhesive layer and/or the interface is an alternative way to introduce crack-arrest features, which includes techniques such as manufacturing an interlocked 0° layer [21], placing a stiffer barrier at the delaminated interface [22], exposing fibers in CFRP substrates as obstacles to fatigue crack propagation [23], or co-curing thermoplastic patches with CFRP substrates [24]. However, these modifications require extra manufacturing steps and the introduction of more interfaces that might compromise the structural reliability.

* Corresponding author.
E-mail address: gilles.lubineau@kaust.edu.sa (G. Lubineau)

https://doi.org/10.1016/j.compositesa.2020.106094
Received 25 April 2020; Received in revised form 8 August 2020; Accepted 22 August 2020
Available online xxx
1359-835/

We can draw inspiration from natural organisms when designing crack-arrest features. As discussed by Ritchie [25], an extrinsic toughening mechanism (extrinsic dissipation means that it is promoted through careful design of the structure, contrary to "intrinsic", which refers to the material properties) may delay the crack growth without modifying the intrinsic properties, leading to a rising crack-resistance curve (R-curve) behavior [25]. In this way, the required energy increases as the crack propagates, creating a more stable fracture process and, as a result, enhancing joint safety. Human bones are a prime example, whereby extrinsic toughening, including ligament bridging at the crack wake and crack deflection [26,27], contributes significantly to fracture resistance.

Dissipation mechanisms similar to those that occur in bones have also been pursued in engineering materials. By controlling the interfaces between constituent parts, previous studies have shown that ligament bridging, crack deflection, and nucleation of secondary cracks can be promoted in laminated structures [28–31]. In a recent work, Maloney and Fleck addressed adhesive bonding of metallic materials for naval applications, and implemented the above concept through the use of a metallic carrier embedded within the bondline [32]. They showed that crack bridging was enabled by controlling interfacial adhesion using non-sticky PTFE films, and thus observed a significant enhancement in the joint toughness [32]. Although the use of a foreign material within the bondline adds to the total weight of the joint and introduces extra manufacturing challenges, enabling extrinsic dissipation through bridging presents a very promising approach to increase the toughness and damage tolerance of adhesive bonded structures.

In this context, we proposed in a recent study an alternative toughening strategy for composite joints that does not require the use of additional foreign material [33]. In particular, the strategy relies on the formation of bridging ligaments within the bondline, as enabled by the careful control of adhesion at the CFRP/epoxy interface. In that same study, we investigated the proposed mechanism using finite element simulations, and the results showed that bridging of adhesive ligaments can successfully increase dissipation and delay crack propagation, thus enhancing the safety of the bonded joints [33]. However, the promising direction that we outlined in that work needs to be validated experimentally in order to ascertain its feasibility.

Therefore, in this work, we assess the strategy proposed in our previous study through experiments carried out on CFRP/epoxy joints in the double cantilever beam (DCB) configuration. To facilitate the formation of bridging ligaments within the adhesive layer, we controlled the interfacial adhesion by imparting distinct surface properties (*i.e.*, surface patterning) through pulsed CO_2 laser irradiation. Surface areas with distinct adhesion properties were alternatively patterned on the top and bottom substrates of CFRP/adhesive joints by varying the pulse fluence. Moreover, baseline conditions for subsequent analyses were established by analyzing the mode I toughness of corresponding uniformly laser-treated surfaces. We show that the number of arrest regions and their spacing largely affects the magnitude and the efficiency of crack bridging, and controls the stability of the crack propagation, compared with the control interfaces. Our detailed study reveals the practical bridging mechanisms and sheds light on the optimum design parameters that produce a reliable adhesively bonded CFRP joint with increased safety.

2. Materials and methods

2.1. Material

Unidirectional laminates ($[0°]_8$) were manufactured by stacking aerospace-grade carbon fiber-reinforced epoxy pre-pregs (HexPly T700/M21, Hexcel, Stamford, CT, USA), which had a nominal fiber volume of 57%. While manually stacking the pre-pregs, a full vacuum (1 bar) was applied twice, once every four-layer stacking, to reduce air entrapment and void formation. The CFRP laminates were cured using a hydraulic hot press machine (Hydraulic presses, Pinette Emidecau Industries, Chalon-sur-Saone, France) under a gauge pressure (7 bar). The heating rate was set to $3°C/min$ and a hold time of 120 min at $180°C$. The laminate was then cooled at a rate of $3°C/min$. Cured unidirectional CFRP laminate has the orthotropic property of E_{xx} = 125000 MPa, $E_{yy} = E_{zz}$ = 7800 MPa, $\nu_{xy} = \nu_{xz}$ = 0.33, ν_{yz} = 0.4, $G_{xy} = G_{xz}$ = 5100 MPa, and G_{yz} = 2786 MPa. Two component epoxy adhesives (Araldite 420 A/B, Huntsman, Salt Lake City, UT, USA) were employed to bond the cured CFRP substrates. The epoxy part and the hardener were mixed with a weight ratio of 10:4. The mixture was then applied to a bonding surface and cured under room temperature for 12 h. The cured epoxy material has a Young's modulus of E = 1500 MPa and Poisson ratio ν = 0.33.

2.2. Surface patterning strategy

Flat baseline surfaces were chosen as the starting stage for laser processing. These surfaces were obtained by covering the CFRP laminates with a Teflon film during curing, which were called *T* [7]. Pulsed laser irradiation was carried out using a 10.6 μm CO_2 laser (PLS6.75 Laser Platform, Universal Laser Systems, NY, USA) to achieve fast and reproducible surface patterning on CFRP plates. Two processing conditions were employed, which featured distinct values of the pulse fluence (F_p). The first processing route was an ablation process that fully exposed carbon fibers, which was carried out at $F_p = 3.6$ J/cm^2. We denoted it as laser ablation (*LA*) in the remainder of this work. A distinct surface condition was achieved at a pulse fluence of $F_p = 1.2$ J/cm^2, and featured minor modifications of surface roughness with partially exposed carbon fibers, whose aim was to clean the surface with minimum removal of surface epoxy. This treatment was denoted as laser cleaning (*LC*). The precise values of laser processing parameters and corresponding SEM observations of *LA* and *LC* surfaces were presented in our previous work [7]. To complete surface preparation, after pulsed CO_2 laser irradiation, the treated surfaces were degreased in an ultrasonic bath of acetone for 10 min, and then dried at $50°C$ for 25 min in the oven before applying the epoxy adhesive. The choice of these surface treatments was informed by our previous work reported in [7,33]. Indeed, based on the observed contrast in cohesive strength of *LC* and *LA* interfaces (*i.e.*, 24.5 versus 19.0 MPa), our modeling approach suggested that the formation of adhesive ligaments and associated extrinsic dissipation would be feasible.

As shown in Fig. 1, *LA* and *LC* pretreatments were deployed homogeneously on CFRP substrates, and DCB adhesive joints were fabricated to establish the baseline fracture properties (*i.e.*, uniform configurations). Subsequently, patterned interfaces were obtained by combining the above treatments. The arrest regions were generated using the laser cleaning surface pretreatment, while the remainder of the surface received a laser ablation outlined above. In the single ligament configuration, the arrest regions displaced by a gap were generated on each of the mating substrates, and are illustrated by the dark green regions in Fig. 1. The size of the arrest region, *i.e.*, the anchor size, and the gap distance, *i.e.*, the distance between consecutive arrest regions, were both set to 5 mm. This single patterning configuration was denoted as *SP*5. Finally, multiple arrest regions were alternatively deployed to both CFRP substrates with a fixed anchor size of 5 mm. Three pattern configurations were realized with gap distances of 2.5, 5, and 10 mm, which were named *MP*2, *MP*5, and *MP*10, respectively.

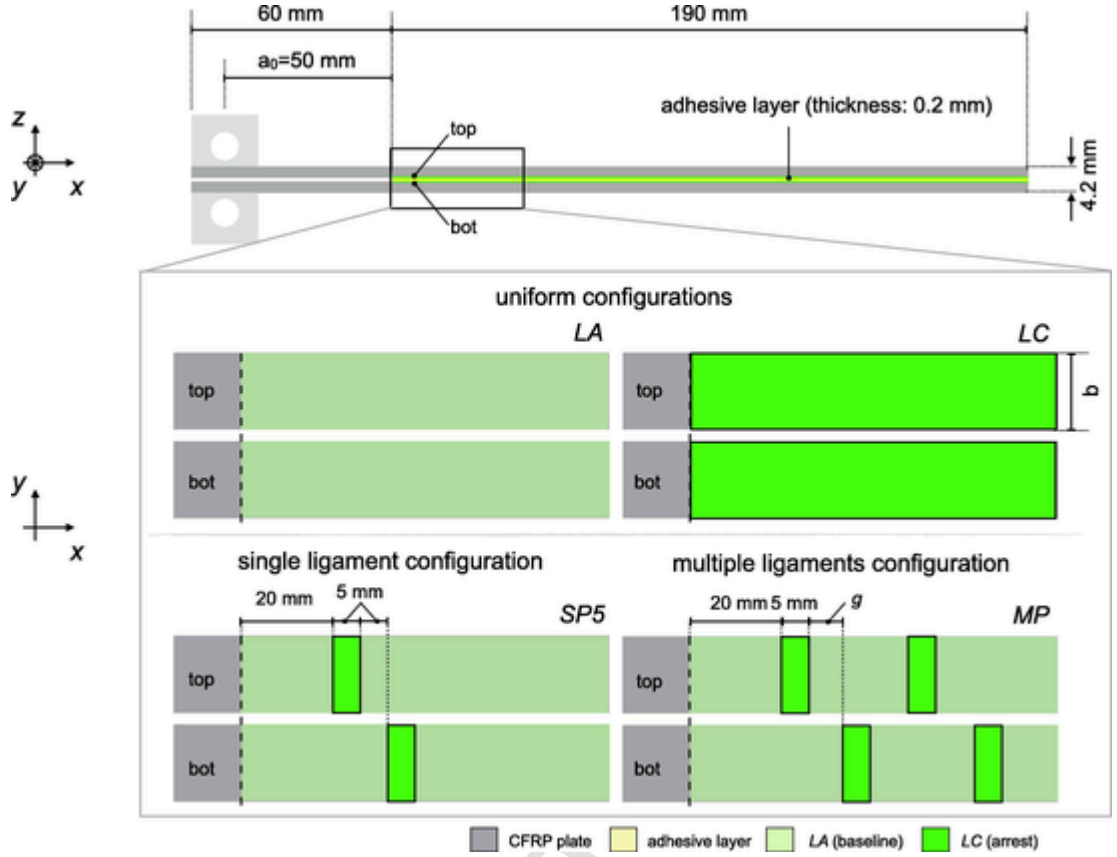

Fig. 1. Schematics of investigated surface pretreatments. The DCB specimen has a width $b = 20$ mm. Two uniformly treated surfaces *LA* and *LC*. The single patterning of *LA* and *LC*, denoted as *SP5*, has the anchor size and gap distance equal to 5 mm. Three different multiple patterns are obtained by changing the gap distance *g* between the adjacent arrest treatments. *MP2*, *MP5*, and *MP10* stand for gap distance of 2.5, 5, and 10 mm, respectively.

2.3. Double cantilever beam tests

Mode I fracture tests were carried out using the DCB configuration according to the procedures and recommendations reported in the ASTM D5528-13 standard ([34]). The CFRP laminates $[0°]_8$ were bonded using the Araldite 420 epoxy adhesive with a nonadhesive polyethylene insert (60 mm long, 0.08 mm thick) as the crack starter. Two mating surfaces were aligned at the end of this insert to ensure the positioning of the laser-based patterning. Since the treatment variability might result in cohesive failure in the case of a thin bondline [35], a thicker adhesive layer, controlled by fishing lines (0.2 mm diameter), was employed here (in contrast to our previous work) to ensure pure interfacial delamination at weak interfaces (*LA*). Mechanical pressure was applied, by using calibrated weights that ensured a uniform pressure of about 0.17 bar, to promote full adhesive-CFRP contact and a consistent thickness of the adhesive layer. The epoxy was cured at room temperature over 12 h in a temperature- and moisture-controlled laboratory environment, *i.e.*, 22 °C and 51% R.H. The bonded CFRP plate was then cut into $250 \times 20 \times 4.2$ mm^3 specimens using a water-jet cutting machine (ProtoMax, Omax, Washington, USA). Finally, aluminum loading blocks were bonded onto each specimen's arm using the same epoxy adhesive to enable the application of the end peel loading.

Mechanical tests were carried out under monotonous displacement control at a rate of 0.5 mm/ min using a universal testing machine (Instron 5882, Instron, Massachusetts, USA). A displacement limit was set up to 75 mm or to final failure of the whole specimen. The crack propagation was observed in situ using a high-resolution camera (Canon EOS-1Ds, resolution 5616 × 3744 pixels) and with the aid of black lines at every millimeter marked on the specimen edge. The energy release rate (ERR, *G*) was calculated based on the compliance calibration (CC) data reduction method [34].

3. Results and discussion

3.1. Effect of arrest regions

Mechanical tests have shown that DCB adhesive joints with uniform laser pretreatments *LA* and *LC* were characterized by average mode I ERR values of 0.28 ± 0.04 and 0.25 ± 0.05 kJ/m^2 under DCB tests, respectively. The typical load–displacement responses and corresponding ERR values of uniform pretreatments are shown in Fig. 2. Both load–displacement curves demonstrate stick–slip behavior, indicating some heterogeneity in the adhesion properties, even though these treatments were defined as being homogeneous. The obtained ERR of *LC* was much more scattered than that of *LA*, varying from 0.20 to 0.38 kJ/m^2. This large variation arose from the high surface heterogeneity, since partially exposed surface carbons may be loosened by the removal of the supporting epoxy resin [36].

A typical load–displacement response and corresponding ERR of *SP5* are illustrated in Fig. 2, where the green area highlights the position of the arrest regions. After applying the single pattern, the crack is arrested and the applied load is substantially increased, while ERR is elevated to twice that of the control surface *LA*, indicating the successful formation of the adhesive ligament. The obtained ERR could be decomposed into the interface detachment part G_d, the request energy for the bridging ligament G_l, and the kinetic part G_k, $G = G_d + G_l - G_k$ [37]. Since G_k was no more than 10% of total ERR *G* under the quasi-static loading condition, it will not be included in the following discussion [37]. The total energy required

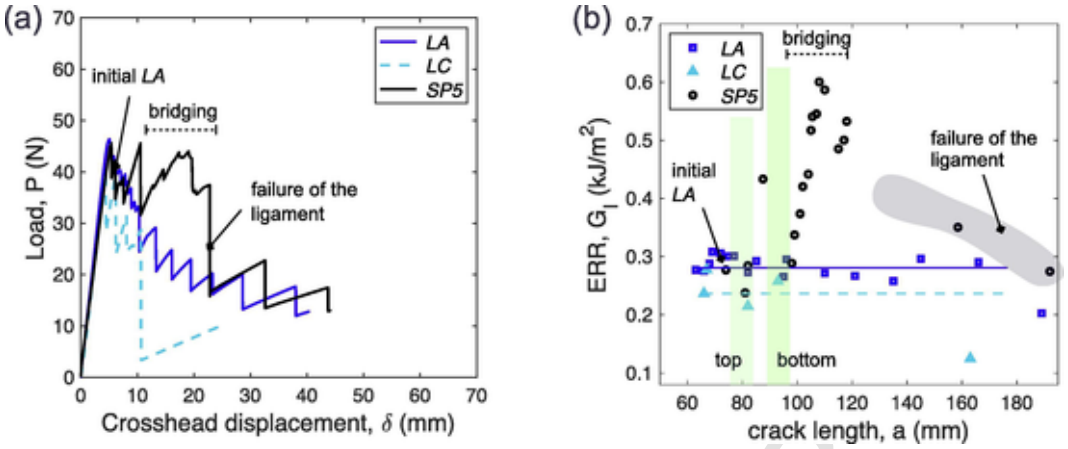

Fig. 2. Typical load–displacement curve and the corresponding ERR of single patterning *SP5*. Typical global responses of uniform *LA* and *LC* are also illustrated for comparison. The dashed lines indicate the regimes with the bridging of adhesive ligaments. The arrest *LC* region is highlighted in green in the R-curve.

for crack propagation (U_t) can be obtained as follows,

$$U_t = \int_{a_0}^{a_f} G(a)bda = \int_{a_0}^{a_f} G_d(a)bda + \int_{a_0}^{a_f} G_l(a)bda, \tag{1}$$

where b is the width of the DCB specimen, and a is the projected crack length. The corresponding values a_0 and a_f are shown in Fig. 3(a). As depicted in Fig. 3(b) and (c), after the primary crack is stopped by the arrest interface (green region) at point 1, a secondary crack is nucleated at the top interface and quickly propagates both backwards (a_2^t) and forwards (a_3^t), thus generating an adhesive ligament (point 2). As the secondary crack propagates at the top interface, the triggered adhesive ligament holds the separating arms and ERR increases displaying an R-curve response. The backward advance (a_2^t) only occurs during the initiation of the secondary crack, which determines the length of the activated ligament (around 3 mm). The projected crack length could be decomposed into $a = a_1^b + a_2^b + a_3^t$, as illustrated in Fig. 3 (c). The obtained U_t includes the energy dissipated from the detachment of the adhesive layer U_d, and the strain energy stored in the adhesive ligament (U_l) prior to failure at $a = a_f$. U_d was estimated to segregate the latter contribution by multiplying the actual delaminated interfacial area by the average toughness $G_{LA} = 0.28$ kJ/m^2, *i.e.*,

$$U_d = \int_{a_0}^{a_f} G_d(a)bda = G_{LA} \cdot b \cdot \tilde{a}, \tag{2}$$

where $\tilde{a} = a_1^b + a_2^b + a_2^t + a_3^t$ is the actual length of the delaminated top and bottom interfaces (Fig. 3(c)). Finally, the interface detachment ERR G_d was calculated by the incremental U_d with respect to the area of projected crack growth,

$$G_d = \frac{\Delta U_d}{b \cdot \Delta a}. \tag{3}$$

Before point 2 depicted in Fig. 3, the total required energy U_t, as integrated from the R-curve, and the dissipated energy of the interface U_d are identical, while G_d illustrates a slight increase due to delamination of both the top and bottom interfaces when initiating the secondary crack. Then, the adhesive ligament is stretched as the crack propagates and the extra elastoplastic energy is stored. Thus, the incremental U_t starts to deviate from the pure dissipation of CFRP/adhesive interfaces up to point 4. If we consider point 2 as the initiation point, the difference between U_t and U_d up to the point of ligament fracture can be as large as ≈75%.

Based on our previous numerical investigations [33], we found that plastic deformation and damage within the adhesive layer was rather limited; thus, a portion of the external energy was stored in the form of elastic energy within the bridging ligament. The experimental observations presented here indeed confirm the sudden release of this stored elastic energy. The occurrence of fast propagation upon fracture of the bridging ligament is denoted by point 4 in Fig. 3. Notice that failure occurs due to the bending and stretching of the ligament, leading to a large drop in the ERR curves. Further note that the arrest region *LC* does not contribute to the ERR, but only in the creation and anchoring of adhesive ligaments.

Optical observation of the fracture surface is also shown in Fig. 3, where the generated adhesive ligament is only half of the total width of the specimen. This fracture surface observation varied between different specimens because *LC* led to randomly distributed loose fibers, which were detrimental to the adhesion [36] and resulted in scattered maximum ERR values.

3.2. Effect of the gap distance in multiple patterning

Mechanical responses of multiple patterning of *LA* and *LC*, as well as corresponding fracture surfaces, are presented in Fig. 4 for different gap distances. Global responses of the single patterning *SP5* is also included for comparison. All four load–displacement curves illustrate a similar response to *LA* at the beginning because of the 30-mm-long control area. The ERR curves share a similar initial stage, corresponding to ERR of *LA*. After that, there is a significant increase that reflects the occurrence of the bridging stage, followed by an apparent stabilization stage (plateau-like), which is highlighted by the shaded area in Fig. 4(b). At the stabilization stage, obtained ERR drops when the stretched adhesive ligaments break while increases again after generating new ones. The average of such fluctuated ERR is illustrated as the dashed line.

When the gap distance was 2.5 mm (*MP2*), three or four ligaments were simultaneously bridging the separating arms, leading to the highest load–displacement curve and enhanced ERR. The average plateau value (shown as the dash line) reached a remarkably high value of 1.01 ± 0.17 kJ/m^2, but the R-curve can potentially reach a maximum value of up to 1.40 kJ/m^2, for example, as shown in Fig. 4. We observed two adhesive ligaments in the bridging of *MP5*, whose maximum value recorded on the R-curve was 0.89 ± 0.07 kJ/m^2.

When the gap distance further increased to 10 mm, the efficiency of ligament bridging, and the corresponding R-curve, was reduced; indeed, only a single ligament was observed in the process zone. Due to surface heterogeneity of the *LC* treatment, the formation of adhesive ligaments was not consistent. A partial ligament could be triggered (cyan arrows on the fracture surfaces in Fig. 4 (c)) or the ar-

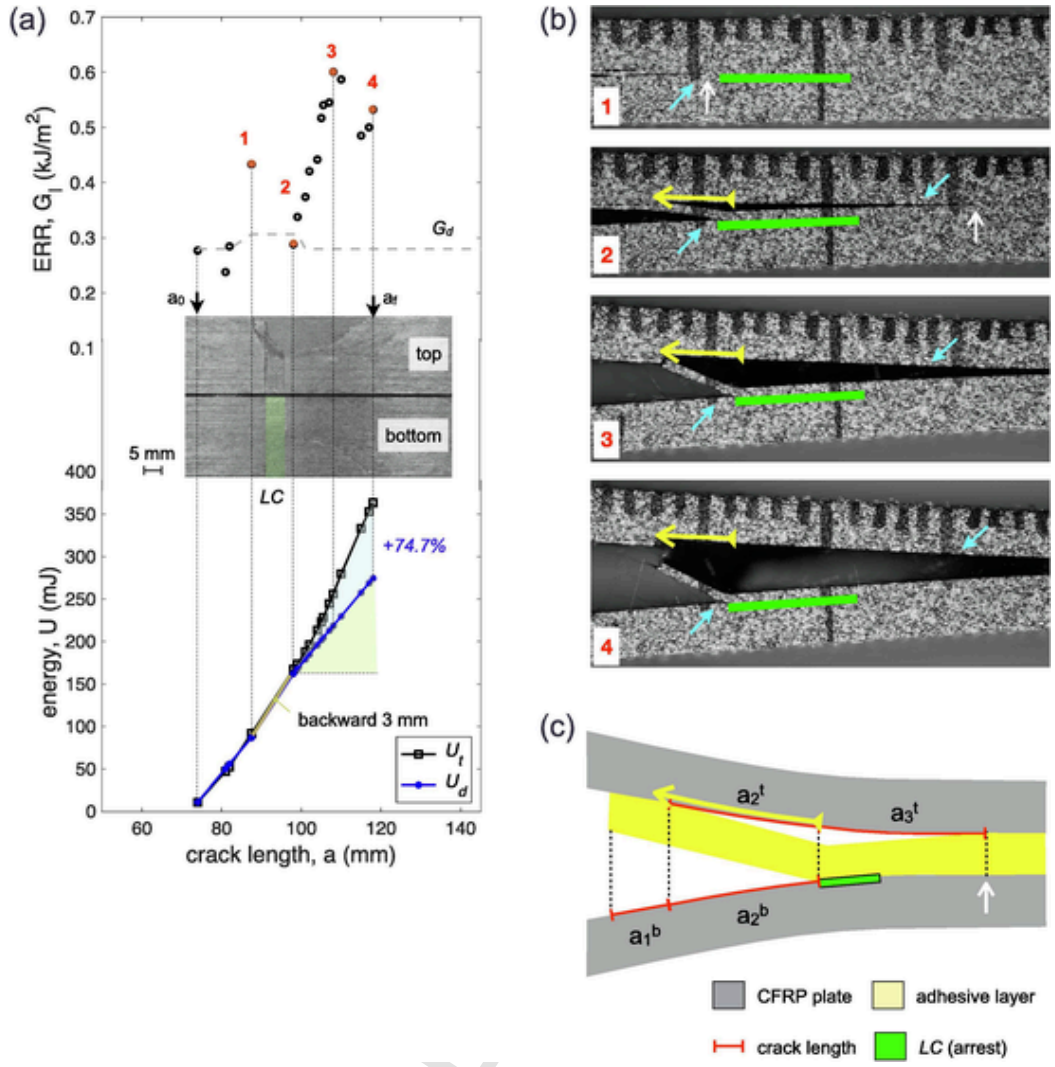

Fig. 3. (a) R-curve, nominal detachment ERR G_d, fracture surface, and integrated energy evolution U_t of *SP*5. The backward crack length is highlighted between point 1 and 2. (b) In situ corresponding crack propagation observed from the side of the DCB specimen. Upward cyan arrows indicate the primary crack, while downward cyan arrows point to the secondary crack on the top CFRP/adhesive interface. The backward crack propagation areas are illustrated in yellow and the arrest regions *LC* are highlighted in green. White arrows point to the location of the crack tip. (c) Schematic of the decomposition of the crack length.

rest interface occasionally failed to generate it (yellow arrows on the fracture surfaces in Fig. 4 (c)). In other specimens of *MP*10, two adhesive ligaments were produced, leading to a similar toughening as *MP*5. Thus, this variation in the number of bridging ligaments gave an average R-curve plateau value of 0.72 ± 0.12 kJ/m^2 for *MP*10.

Comparison of the total required energy, U_t, and the interfacial dissipated energy, U_d, of *MP*2 is depicted in Fig. 5, along with the in situ snapshots of crack propagation. Since this energy comparison of *MP*2, *MP*5, and *MP*10 induced similar observations, here we discuss only that of *MP*2. After initiating at point 1, a large-scale bridging phenomena occurs, as illustrated in Fig. 5. The increased part of the obtained R-curve is approx. 22 mm in size, representing a progressively expanded bridging zone comprising up to three ligaments holding the crack faces at the same time. Then, the R-curve reaches a peak at point 3 followed by a slight ERR drop because only a partial ligament was created (see corresponding fracture surface). Moreover, due to the small gap distance (2.5 mm), the bridging ligament can be peeled off in a backward motion to the previous arrest region located on the opposite interface, as highlighted by the red circle in Fig. 5. A larger enhancement is observed at point 6, because four ligaments are in function simultaneously. Finally, the breakage of ligaments occurs at point 7 and catastrophic failure follows. Starting from point 1, the incremental U_t largely increases and deviates from the dissipation of the CFRP/adhesive interfaces, ending up with being 162.9% higher than U_d (*i.e.*, $(\Delta U_t - \Delta U_d)/\Delta U_d = 162.9\%$). Since the plastic and damage dissipation of the adhesive layer was limited, the majority of the enhanced energy was stored as elastic energy in the bridging adhesive ligaments. A similar conclusion can be drawn based on the nominal detachment ERR G_d, which exhibited a slight increase after point 1 and then fluctuated due to the varying length of the generated adhesive ligaments.

In summary, triggered adhesive ligaments may significantly promote ERR in the investigated DCB joint system, and an increase in bridging ligaments led to a higher plateau value of the obtained R-curve. Two mechanisms were responsible for this enhancement. First of all, the bridging ligaments created multiple damaged interfaces, thus slightly increasing the ERR values when the crack propagated. More importantly, as shown in the comparison of the integrated required energy U_t and the interfacial dissipated energy U_d, a large amount of strain energy was required when bending and stretching multiple adhesive ligaments while propagating the crack. A large portion of this energy was suddenly released and led to fast crack propagation when the ligament failed.

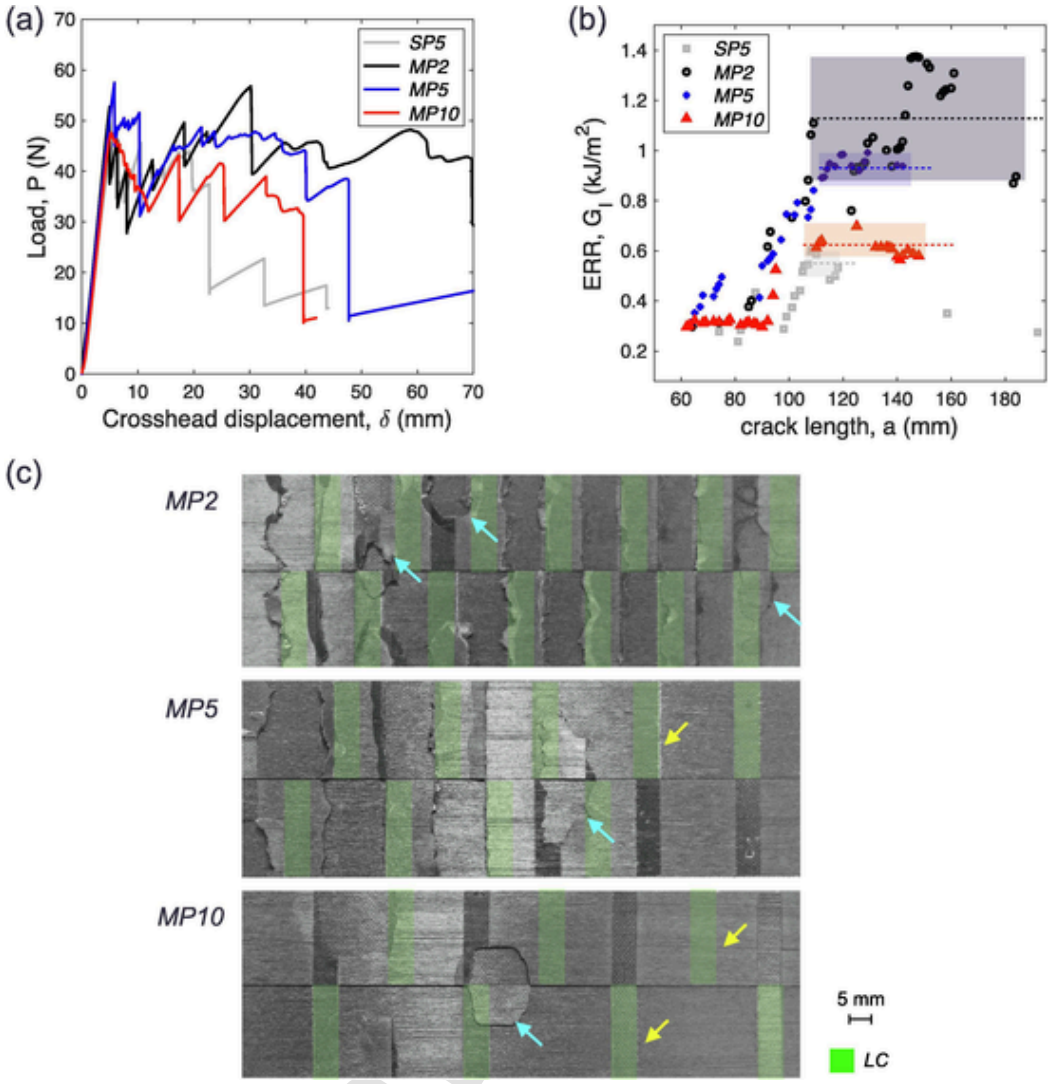

Fig. 4. (a) Typical load–displacement curve and (b) the corresponding ERR of multiple patterning *MP2*, *MP5*, and *MP10*. Shaded areas highlight the stabilization stage and dashed lines indicate the average ERR within this stage. Typical global responses of *SP5* are also illustrated for comparison. (c) Fracture surfaces of multiple patterning *MP2*, *MP5*, and *MP10*. Cyan arrows point to the partial adhesive ligaments and yellow arrows indicate the positions that failed to trigger ligaments.

3.3. Effect of scattered LC ERR

As described earlier, adhesive ligaments may be partially triggered or even absent. This can be explained by the variation in surface conditions of *LC*, which is associated with the occurrence of partially exposed fibers [36], leading to fairly large fluctuations in the obtained ERR of uniform *LC* interfaces, *e.g.*, from 0.20 to 0.38 kJ/m^2. We carried out finite element (FE) simulations to further explore this point, through a two-dimensional FE model of the DCB sample (ABAQUS, Simulia, Johnson, RI, USA). We used cohesive elements to simulate interfacial failure at the top and bottom interfaces. The detailed description of the FE model was provided in our previous work [33].

In the current FE model, the adhesive thickness was set to 0.2 mm, and the geometrical arrangement of *LA* and *LC* interfaces was reproduced through the spatial assignment of cohesive zone input properties. *LA* was the control surface with an interfacial strength of 19 MPa [36] and the fracture toughness of 0.28 kJ/m^2 that was obtained earlier. At the arrest region, the interfacial strength of *LC* was 24.5 MPa [36], while we considered two values of fracture toughness in the analysis to account for the variability of adhesion properties, *i.e.*, 0.20 and 0.38 kJ/m^2.

The obtained global load–displacement and R-curve responses were similar to experimental results in both cases, as depicted in Fig. 6. However, the local damage mechanisms of the bridging ligament were different. When the arrest region had a smaller toughness value, *i.e.*, $G_{LC} = 0.20 < G_{LA}$, the ligament delaminated from the arrest region, as shown in both experimental and numerical results in Fig. 6 (c), while higher toughness of the arrest region ($G_{LC} = 0.38 > G_{LA}$) stopped the crack advance and led to the backward delamination at the top interface (Fig. 6 (f)). The results suggest that interfacial strength plays a much more critical role on the formation of adhesive ligaments. Indeed, the precise mismatch in toughness seems to be of secondary importance, being the conditions $G_{LC} > G_{LA}$ or $G_{LC} < G_{LA}$ equally able to trigger a ligament with minor modification in the overall dissipation.

To achieve more repeatable bridging ligaments, the same laser-based *LA* and *LC* were applied to rough baseline surface *PP*, which we obtained by covering a nylon peel-ply (*PP*) film on top of stacking pre-pregs while curing CFRP laminates, achieving a multi-patterning of *PPLA* and arrest regions *PPLC*. The surface profiles, obtained by contact profilometry (Dektak 150 Surface Profiler, Veeco,

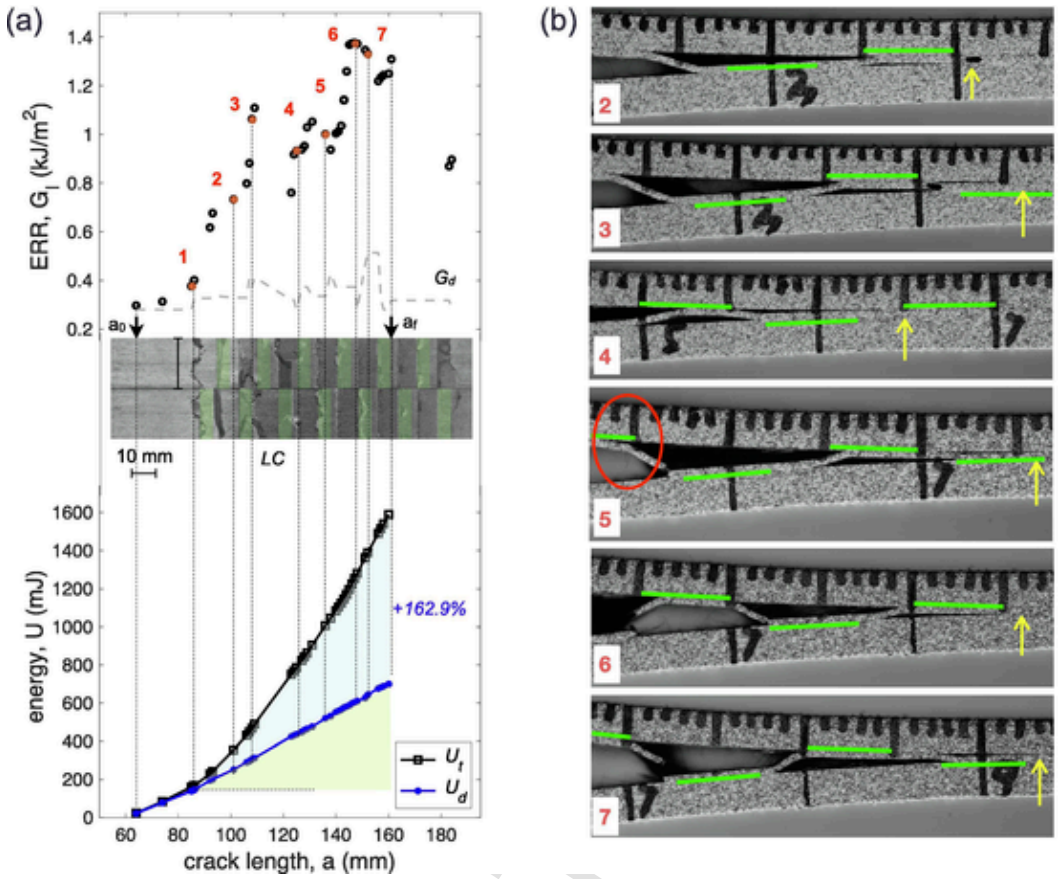

Fig. 5. (a) R-curve, nominal detachment ERR G_d, fracture surface, and integrated energy evolution U_t of *MP2*. (b) In situ corresponding crack propagation observed from the side of the DCB specimen. The arrest regions *LC* are highlighted in green and yellow arrows indicate positions of the crack tip.

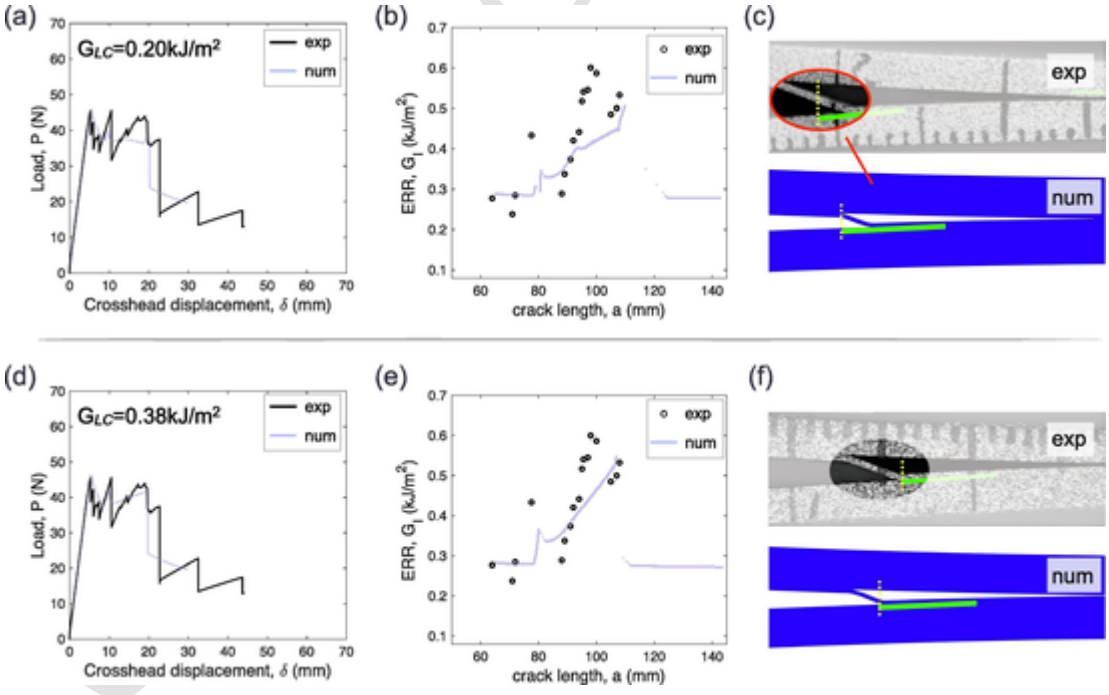

Fig. 6. Comparison between experimental responses and numerical results using two cohesive fracture toughness values of the arrest region. The selected toughness values are the lowest and the highest values obtained from uniform *LC*, (a) Load–displacement curves, (b) corresponding R-curves, and (c) local damage observations of 0.20 kJ/m^2, while (d) load–displacement curves, (e) corresponding R-curves, and (f) local damage observations of 0.38 kJ/m^2. Dashed yellow lines in (c) and (f) highlight the beginning of the arrest regions, which are illustrated in green.

New York, USA), showed that the laser treatment on flat CFRP surface did not introduce significant variations in the surface morphology. However, the *PPLC* surface, as shown in Fig. 7, still featured the original large roughness associated with the peel ply texture ($S_a = 12.32 \pm 2.15\ \mu$m), while *PPLA* showed a much lower roughness of $S_a = 4.33 \pm 1.40\ \mu$m. We believe that this morphology difference aided the formation of adhesive ligaments. We thus evaluated the contribution of such morphology variation by deploying the proposed laser-based patterning on DCB configurations, with an arrest interface of 5 mm and gap distance of 5 mm. The fracture surfaces of the tested specimens are illustrated in Fig. 8, along with the corresponding schematic of the surface patterning. The dash lines clearly indicate the locations of the broken adhesive ligaments, with a spacing distance of 10 mm. When the crack front met the arrest region *PPLC*, for example at point *a* in Fig. 8, a secondary crack was initiated at the opposite surface, *i.e.*, at point *b*, and the full adhesive ligament was generated. Thus, the height difference of the patterning on *PP* surfaces proved to be sufficient to achieve stable and controllable ligament formation.

4. Conclusions

In this work, we experimentally assessed an innovative damage-tolerant interfacial design concept for CFRP/epoxy joints. The proposed design relies on extrinsic dissipation enabled by crack bridging of adhesive ligaments directly formed within the bondline of the joint, *i.e.*, without the need to include any additional foreign material. We generated surface patterns, *i.e.*, areas with distinct adhesion properties, over CFRP substrates by tuning the fluence of a pulsed CO_2 laser beam. We carried out DCB tests in conjunction with high-resolution in situ imaging of the fracture process to ascertain the fracture behavior of the joint, and to shed light on the mechanisms of adhesive ligament bridging.

The experimental results indicated that our proposed strategy showed substantial potential both for the generation of adhesive ligaments and to increase the joint toughness through large-scale bridging phenomena. We observed a major enhancement in the obtained ERR resulting from the strain energy stored in bending and stretching the adhesive layer. A patterned interface with spacing of around 2.5 mm led to the highest average plateau value of the obtained R-curve for the studied material system. In particular, increased bridging adhesive ligaments affected the fracture process, by storing more elastic energy during propagation of the crack. Moreover, the mechanical tests showed very good correlation with our previous finite element investigation. However, the results also highlighted the sensitivity of the bridging phenomena to local heterogeneities in the laser-treated surfaces, which may lead to an increase in experimental scatter in the recorded mechanical responses. However, this issue did not compromise the effectiveness of our method. We have also outlined that the large scattering can be effectively reduced by applying the laser-based patterning on a rough baseline surface. By electing a peel-ply surface to assess this point experimentally, we have shown that the robustness of the proposed patterning strategy in terms of effective deployment of ligament bridging can be substantially improved. More complex surface patterning strategies, prepared using

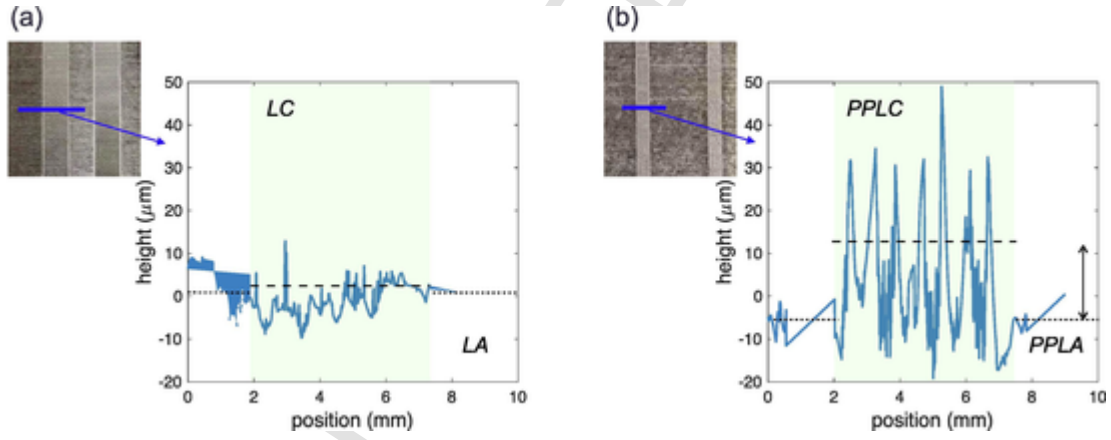

Fig. 7. Optical observation and corresponding surface profiles of *LA/LC* and *PPLA/PPLC* patterning. The highlight regions are the arrest region *LC* with a size of 5 mm. Dashed lines show the average profile heights of *LC* and *PPLC*, while dotted lines illustrate those of *LA* and *PPLA*. The height difference between *PPLC* and *PPLA* is highlighted by the vertical double arrow.

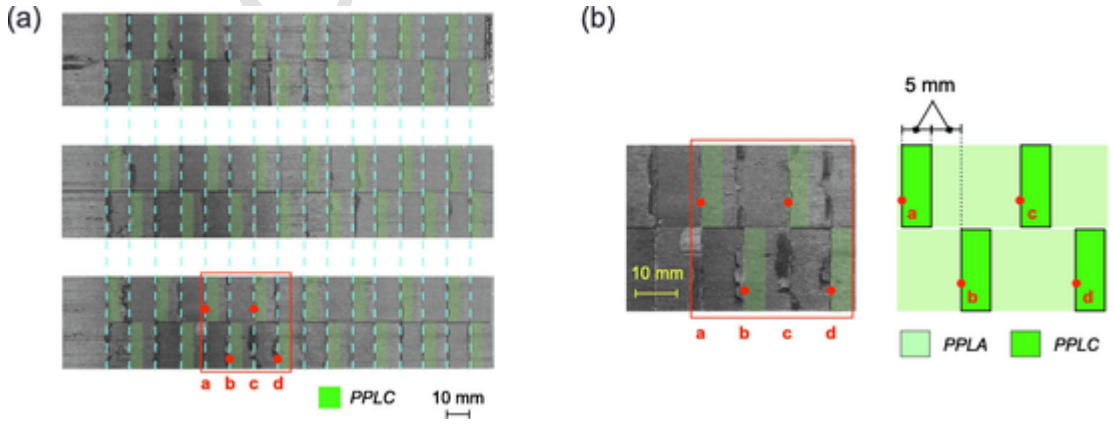

Fig. 8. (a) Fracture surfaces of DCB specimens with *PPLA/PPLC* patterning. Dash cyan lines highlight the breakage location of the adhesive layer. The arrest regions *PPLC* are highlighted in green. (b) Zoomed fracture surface in the red box and corresponding schematic of the surface patterning in the chosen region.

various surface preparation techniques, should be further investigated to trigger adhesive ligaments in different configurations, thereby paving the way for reliable and safe adhesively bonded composite joints.

5. Data availability

The datasets generated during and/or analyzed during the current study are available from the corresponding author on reasonable request.

6. Author contribution

G.L, M.A. and A.Y.: Conceptualization, Methodology, Supervision R.T. and X.L.: investigation, Data Curation All authors: Writing - Original Draft, Writing - Review and Editing.

Declaration of Competing Interest

The authors declare no financial or non-financial competing interests.

CRediT authorship contribution statement

Ran Tao: Investigation, Data curation, Writing - original draft, Writing - review & editing. **Xiaole Li:** Investigation, Data curation. **Arief Yudhanto:** Conceptualization, Methodology, Supervision, Writing - original draft, Writing - review & editing. **Marco Alfano:** Conceptualization, Methodology, Supervision, Writing - original draft, Writing - review & editing. **Gilles Lubineau:** Conceptualization, Methodology, Supervision, Writing - original draft, Writing - review & editing.

Declaration of Competing Interest

The authors declare that they have no known competing financial interests or personal relationships that could have appeared to influence the work reported in this paper.

Acknowledgement

The research reported in this publication was supported by funding from King Abdullah University of Science and Technology (KAUST) Office of Sponsored Research (OSR) under award number OSR-2017-CRG6-3388.01.

References

[1] T. Schmid Fuertes, T. Kruse, T. Körwien, M. Geistbeck Bonding of CFRP primary aerospace structures, a discussion of the certification boundary conditions and related technology fields addressing the needs for development. Compos Interfaces 2015;22(8):795–808.
[2] P. Galvez, A. Quesada, M. Martinez, J. Abenojar, M. Boada, V. Diaz Study of the behaviour of adhesive joints of steel with CFRP for its application in bus structures. Compos Part B: Eng 2017;129:41–46.
[3] P. Ladevéze, G. Lubineau On a damage mesomodel for laminates: micro–meso relationships, possibilities and limits. Compos Sci Technol 2001;61(15):2149–2158.
[4] Y.W. Kwon, D.H. Allen, R. Talreja Multiscale modeling and simulation of composite materials and structures, Vol. 47. Springer; 2008.
[5] D. Markatos, K. Tserpes, E. Rau, S. Markus, B. Ehrhart, S. Pantelakis The effects of manufacturing-induced and in-service related bonding quality reduction on the mode-I fracture toughness of composite bonded joints for aeronautical use. Compos Part B: Eng 2013;45(1):556–564.
[6] K. Katnam, L. Da Silva, T. Young Bonded repair of composite aircraft structures: A review of scientific challenges and opportunities. Prog Aerosp Sci 2013;61:26–42.
[7] R. Tao, M. Alfano, G. Lubineau Laser-based surface patterning of composite plates for improved secondary adhesive bonding. Compos Part A: Appl Sci Manuf 2018;109:84–94.
[8] S. Prolongo, M. Gude, G. Del Rosario, A. Ureña Surface pretreatments for composite joints: study of surface profile by SEM image analysis. J Adhes Sci Technol 2010;24(11–12):1855–1867.
[9] E.P. Chan, A. Dongchan, A.J. Crosby Adhesion of patterned reactive interfaces. J Adhes 2007;83(5):473–489.
[10] M. Budzik, J. Jumel, K. Imielińska, M. Shanahan Fracture in composite/aluminium joints of variable adhesive properties. J Adhes 2009;85(10):736–754.
[11] S. Patinet, L. Alzate, E. Barthel, D. Dalmas, D. Vandembroucq, V. Lazarus Finite size effects on crack front pinning at heterogeneous planar interfaces: Experimental, finite elements and perturbation approaches. J Mech Phys Solids 2012;61(2):311–324.
[12] S. Xia, L. Ponson, G. Ravichandran, K. Bhattacharya Adhesion of heterogeneous thin films II: Adhesive heterogeneity. J Mech Phys Solids 2015;83:88–103.
[13] S.R. Ranade, Y. Guan, R.B. Moore, J.G. Dillard, R.C. Batra, D.A. Dillard Characterizing fracture performance and the interaction of propagating cracks with locally weakened interfaces in adhesive joints. Int J Adhes Adhes 2018;82:196–205.
[14] C. Cuminatto, G. Parry, M. Braccini A model for patterned interfaces debonding–application to adhesion tests. Int J Solids Struct 2015;75:122–133.
[15] S. Heide-Jørgensen, M.K. Budzik Effects of bondline discontinuity during growth of interface cracks including stability and kinetic considerations. J Mech Phys Solids 2018;117:1–21.
[16] K. Tserpes, G. Peikert, I. Floros Crack stopping in composite adhesively bonded joints through corrugation. Theoret Appl Fract Mech 2016;83:152–157.
[17] P. Chang, A. Mouritz, B. Cox Properties and failure mechanisms of pinned composite lap joints in monotonic and cyclic tension. Compos Sci Technol 2006;66(13):2163–2176.
[18] K.T. Tan, N. Watanabe, Y. Iwahori Experimental investigation of bridging law for single stitch fibre using interlaminar tension test. Compos Struct 2010;92(6):1399–1409.
[19] A. Yudhanto, G. Lubineau, I.A. Ventura, N. Watanabe, Y. Iwahori, H. Hoshi Damage characteristics in 3d stitched composites with various stitch parameters under in-plane tension. Compos Part A: Appl Sci Manuf 2015;71:17–31.
[20] J. Hoffmann, G. Scharr Mode i delamination fatigue resistance of unidirectional and quasi-isotropic composite laminates reinforced with rectangular z-pins. Compos Part A: Appl Sci Manuf 2018;115:228–235.
[21] S. Minakuchi Fiber-reinforcement-based crack arrester for composite bonded joints. 20th ICCM; 2015.
[22] H. Matsuda, G. Matsubara, A. Kuraishi, Y. Hirose, M. Hojo Effect of crack arrester on fatigue crack growth in foam core sandwich panel under mode i type loading. Compos Part A: Appl Sci Manuf 2014;56:36–43.
[23] Kruse T, Koerwin T, Heckner S, Geistbeck M. Bonding of CFRP primary aerospace structures - crackstoppings in composite bonded joints under fatigue. In: ICCM 20 20th International Conference on Composite Materials (July); 2015. p. 19–24.
[24] T. Löbel, D. Holzhüter, M. Sinapius, C. Hühne A hybrid bondline concept for bonded composite joints. Int J Adhes Adhes 2016;68:229–238.
[25] R.O. Ritchie The conflicts between strength and toughness. Nat Mater 2011;10(11):817–822.
[26] R. Wang, H.S. Gupta Deformation and fracture mechanisms of bone and nacre. Annu Rev Mater Res 2011;41:41–73.
[27] U.G. Wegst, H. Bai, E. Saiz, A.P. Tomsia, R.O. Ritchie Bioinspired structural materials. Nat Mater 2015;14(1):23–36.
[28] A.C. Orifici, P. Wongwichit, N. Wiwatanawongsa Embedded flaws for crack path control in composite laminates. Compos Part A: Appl Sci Manuf 2014;66:218–226.
[29] S.M.M. Valashani, F. Barthelat A laser-engraved glass duplicating the structure, mechanics and performance of natural nacre. Bioinspir Biomimet 2015;10(2):026005.
[30] S. Goutianos, B.F. Sørensen Fracture resistance enhancement of layered structures by multiple cracks. Eng Fract Mech 2016;151:92–108.
[31] R. Sills, M. Thouless Cohesive-length scales for damage and toughening mechanisms. Int J Solids Struct 2015;55:32–43.
[32] K. Maloney, N. Fleck Toughening strategies in adhesive joints. Int J Solids Struct 2019;158:66–75.
[33] R. Tao, X. Li, A. Yudhanto, M. Alfano, G. Lubineau On controlling interfacial heterogeneity to trigger bridging in secondary bonded composite joints: An efficient strategy to introduce crack-arrest features. Compos Sci Technol 2020;188:107964.
[34] Standard test method for mode I interlaminar fracture toughness of unidirectional fiber-reinforced polymer matrix composites, ASTM Internat; 2014.
[35] X. Li, R. Tao, M. Alfano, G. Lubineau How variability in interfacial properties results in tougher bonded composite joints by triggering bridging. Int J Solids Struct 2020;191–192:87–98.
[36] R. Tao, M. Alfano, G. Lubineau In situ analysis of interfacial damage in adhesively bonded composite joints subjected to various surface pretreatments. Compos Part A: Appl Sci Manuf 2019;116:216–223.
[37] S. Heide-Jørgensen, S.T. de Freitas, M.K. Budzik On the fracture behaviour of CFRP bonded joints under mode I loading: Effect of supporting carrier and interface contamination. Compos Sci Technol 2018;160:97–110.